

Femtosecond laser writing of three-dimensional photonic crystals in polymer

Min Gu* and Guangyong Zhou

Centre for Micro-Photonics and Centre for Ultrahigh-bandwidth Devices for Optical Systems,
Faculty of Engineering and Industrial Sciences, Swinburne University of Technology, Hawthorn,
Victoria 3122, Australia

ABSTRACT

Submicron-sized voids and void channels can be generated in a solid transparent polymer by using a tightly focused femtosecond laser induced micro-explosion method. By stacking the voids and void channels layer by layer and periodically, we can fabricate various three-dimensional (3D) photonic crystals of woodpile, face-centred-cubic, body-centred-cubic, and diamond lattice structures. The photonic bandgap effects and the defect generation in the photonic crystals have been revealed.

Keywords: photonic crystal, microexplosion, polymer; planar cavity

1. INTRODUCTION

Three-dimensional (3D) photonic crystals hold a key to the successful development of all-optical devices. The fabrication of 3D photonic crystals with bandgaps in the infrared or the visible spectral regions is still a challenge for micro-fabrication, as they require a highly correlated arrangement of structural elements at a size of only a few hundred nanometers. Semiconductor etching method is efficient for fabrication of two-dimensional (2D) photonic crystals, but very complicated to fabricate 3D photonic crystals [1,2]. Self-assembling of latex colloids and its inverse structures templating have been used to fabricate 3D photonic crystals. The shortcomings of this method are uncontrollable defects and the limitation of the structures due to the nature properties of self-assembling [3,4]. Two-photon polymerization is a good method to fabricate 3D photonic crystals of numerous lattice types [5,6], but the inherent shrinkage of the polymers upon chemical post etching results in undesirable structural changes to the lattices causing malformation of bandgaps.

By tightly focusing ultrafast laser light into transparent solid materials, micro-explosion occurs at the focal point, where the material is ejected from the centre forming a void cavity surrounded by a region of compacted material [7-9]. If the sample is translated through the focus, micro-void channels featuring elliptical cross sections perpendicular to the channel axis with smooth, well-defined boundaries can be generated [10,11]. This technique has been proved to be efficient to fabricate 2D and 3D void-based photonic crystals, which is a one-step technique and does not require chemical post processing and results in high quality void spheres and void channels. In this paper, we report the fabrication of the void-channel and void-dot based 3D photonic crystals in a solid polymer material by using this microexplosion technique.

2. EXPERIMENTAL

Fig. 1 shows the experimental setup [10]. A 710 nm femtosecond pulsed beam from a 5 W pumped mode-locked Ti:sapphire laser (Mira 900-F; Coherent, Santa Clara, CA) passed through an optical parametric oscillator (Mira-OPO, Coherent; 1065-1265 / 545-625 nm) with an intracavity optical frequency doubler. The resulting beam of wavelength 540 nm had a repetition rate of 76 MHz and a pulse width of 200 fs. A neutral density filter (ND) introduced into the beam path allowed for adjustments in beam intensity. The telescope arrangement led to uniform illumination over the

* mgu@swin.edu.au; phone 61-3-9214 8776; fax 61-3-9214 5435; <http://www.swinburne.edu.au/feis/cmp/>

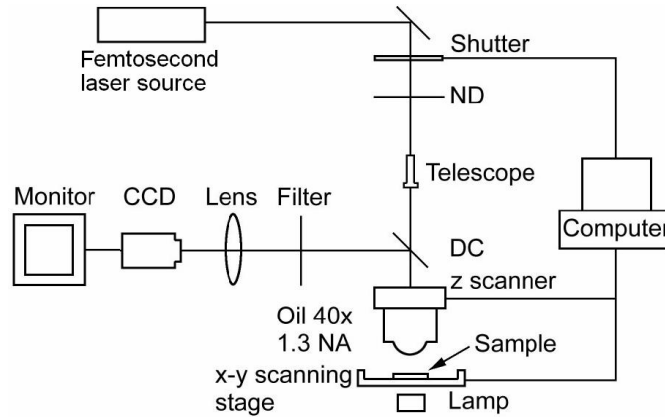


Fig. 1. Optical setup for microfabrication using a femtosecond-pulsed light source. A magnification factor 40, 1.3 NA oil immersion objective focuses the light inside a solidified sample of polymer resin. In-plane translation is controlled by an x - y scanning stage. Moving the objective using a piezoelectric translator controls layer stacking. Fabrication is monitored *in situ* using a CCD camera. ND, neutral density filter; DC, dichroic mirror.

back aperture of an oil immersion objective, Zeiss Plan-Neofluar 40 \times , with numerical aperture 1.3. The sample was mounted on a 200 $\mu\text{m}\times$ 200 μm piezoelectric scanning stage (Physik Instrumente, Waldbronn, Germany) for the in-plane motion, whereas the layer spacing was controlled using a 350 μm piezoelectric translator for the objective (Physik Instrumente). Both the translators and the shutter were computer controlled, and the entire fabrication process was monitored *in situ* by a charge coupled device (CCD) camera gathering the transmission illumination from a halogen lamp beneath the sample as well as fluorescence emission in the focus. The polymerizable material used was Norland NOA 63 resin, which is a polyurethane oligomer having C=C unsaturation and is crosslinked by a mercapto-ester oligomer. The curing process involved exposure of a film of liquid resin sandwiched between glass coverslips to a focused wide band UV light source for a period of 2 hours resulting in a transparent, hard polymer with a refractive index of \sim 1.56.

The photonic band gap were measured by using a Nicolet Nexus Fourier transform infrared (FTIR) spectrometer fitted with a 32 \times , NA 0.65 reflective objective (Reflechromat, Thermo Nicolet, Madison, WI, USA) which provides an incident hollow light cone with an outer angle of 40 $^\circ$ and an inner angle of 15 $^\circ$. To reduce the range of the angle of incidence, a small off-center aperture corresponding to a half angle of 5 $^\circ$ was placed in front of the FTIR objective. Illumination in the [100] crystal direction was achieved by tilting the sample perpendicular to the resulting incidence light cone [12].

3. VOID-CHANNEL-BASED WOODPILE PHOTONIC CRYSTALS

3.1. Generation of void channels inside thin solid polymer films

Continuous, smooth and well-defined micro-void channels can be fabricated when the laser power is above the micro-explosion threshold [10], as shown in Fig. 2(a). Fig. 2(b) shows the ability of fabricating arbitrary shape of channels. To view the cross-section of the void channels, we scanned the laser beam across the surface of the polymer film resulting in a hole on the surface. Fig. 2(c) shows the scanning electron microscopy (SEM) image of void channels fabricated at an average laser power of 20 mW at a scan speed of 60 $\mu\text{m}/\text{s}$ [13]. One can see clearly that the lateral channel diameter is approximately 800 nm. As seen by the bright halo surrounding the void channel, a strongly compressed material region extends a few hundred nanometers away from the channel. In these regions, the density can be increased by as much as 20–50% dependent on structural parameters and fabrication conditions. The densification goes along with an increase refractive index of 5–10% in the polymer [11]. The size of the channel depends on the laser power and the scanning speed. In general, the higher the laser power and the lower the scanning speed, the larger the channels. Also, the laser power and scanning speed strongly determine the quality of the channels [10].

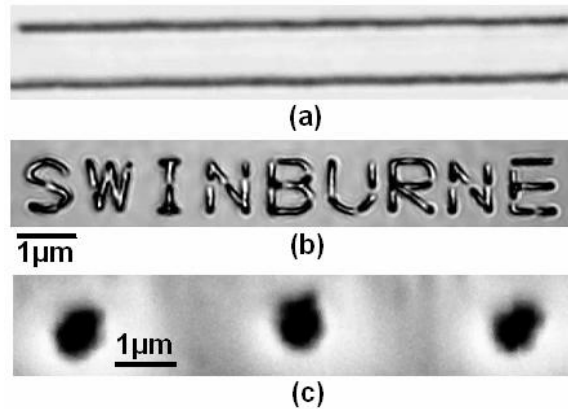


Fig. 2. (a) Transmission microscopy image of smooth void channels and (b) micron-sized letter; (c) scanning electron microscopy image of the cross section of the void channels.

3.2 High quality woodpile photonic crystals with a multitude of higher-order stop gaps

Void channels can be stacked in a woodpile structure type arrangement, as shown in Fig. 3a. Fig. 3b presents the infrared transmission spectrum as measured in the stacking direction for a 20-layer structure with a layer spacing $\delta z=1.6 \mu\text{m}$ and an in-plane channel spacing $\delta x=1.2 \mu\text{m}$ (lateral size $80\mu\times 80 \mu\text{m}$, average laser power 14 mW, scan speed 300 mm/s). The channel diameters are 750 nm and 1.125 μm in the lateral and focussing (stacking) directions, respectively. The fundamental stop gap at 4.6 μm provides a strong suppression of transmission of as much as 86%, and a first higher-order gap at 2.35 μm is observed still yielding a suppression of transmission of 43%. The higher order stop gaps are more visible in the reflection spectra. Fig. 3(c) shows the up to three higher order gaps for a photonic crystal with $\delta z=2.55 \mu\text{m}$ and $\delta x=1.28 \mu\text{m}$. Experimental results show that the layer spacing determines the bandgap position while the in-plane spacing determines the strength of the higher orders. In general, the smaller the in-plane spacing, the stronger the higher order bandgaps.

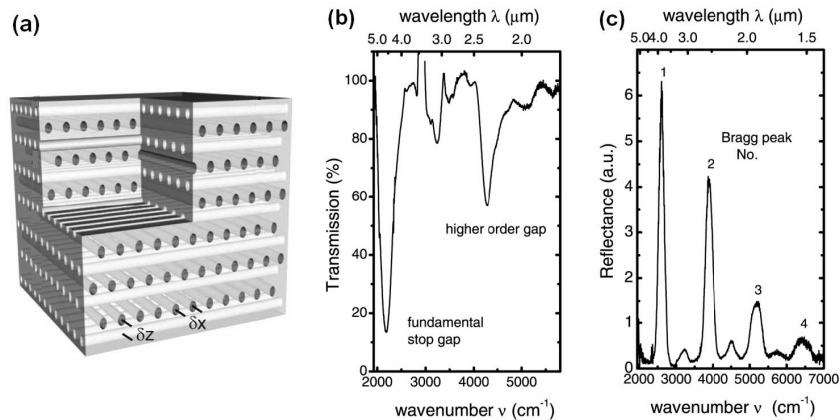


Fig. 3. Sketch of a void channel woodpile structure. Channels are elongated in the focusing (stacking) direction. (b) Transmission infrared spectrum of a sample at $\delta z=1.6 \mu\text{m}$, $\delta x=1.2 \mu\text{m}$. (c) Reflection spectrum of a sample at $\delta z=2.55 \mu\text{m}$, $\delta x=1.28 \mu\text{m}$.

3.3 Planar cavity modes in woodpile photonic crystals

An all-optics chip is supposed to consist of various functional devices such as waveguides with sharp bends [14,15], superprism-based wavelength division multiplexers [16,17] and optical switches which rely on local nonlinearities [18-

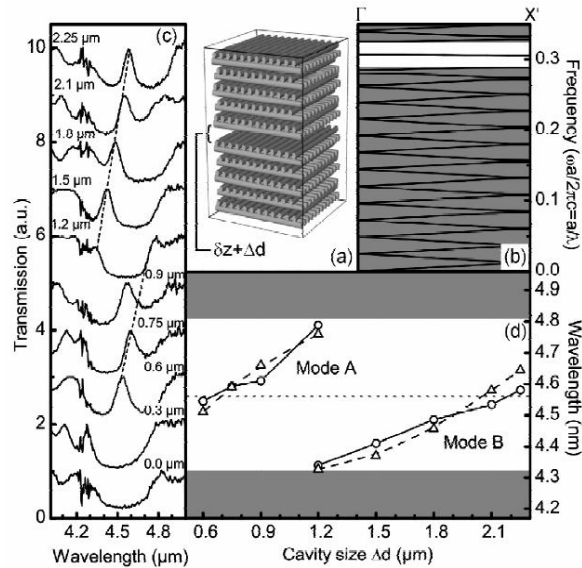


Fig. 4. (a) Sketch of a twenty four-layer void channel woodpile structure with a micro-cavity of size Δd in its centre. (b) Supercell calculation of photonic bands for a structure with a cavity size Δd of 2.1 μm . Shaded regions are frequencies outside the bandgap. The flat band within the bandgap denotes the cavity mode. (c) Infrared transmission spectra in the stacking direction for Δd from 0.3 to 2.25 μm . (d) Variation of experimental (circles) and calculated (triangles) cavity mode wavelengths with the cavity size.

20]. Planar micro-cavity in photonic crystals [21,22] are an important defect category which holds a particular promise upon combination with gain media and are key elements of photonic crystal micro-lasers [23–25]. Planar defect modes have been observed in self-assembled colloidal photonic crystals and two-photon polymerized photonic crystals. Here we demonstrate the functionality of Fabry-Perot type planar micro-cavities with cavity spacings between 0.3 and 2.25 μm in void channel-based woodpile photonic crystals. With increasing cavity size two successive modes emerge from the air band, cross the entire bandgap, and finally disappear in the dielectric band along with characteristic changes in the mode profiles

Micro-cavities were fabricated at the centre of a twenty-four layer woodpile structure with $\delta z=1.5 \mu\text{m}$ and $\delta x=1.4 \mu\text{m}$ by the introduction of a displacement Δd of all layers beyond the twelfth [Fig. 4(a)]. Such a system is analogous to a Fabry-Perot etalon consisting of two parallel quarter-wave stacks [26]. Fig. 4(b) shows the band diagram for $\Delta d=2.1 \mu\text{m}$, where the shaded areas denote frequencies outside the main photonic stop gap in the stacking direction. Within the stop gap a flat band at normalized frequency 0.306 (4.57 μm) demonstrates the existence of a localised defect mode. A series of planar micro-cavities were fabricated with Δd ranging from 0.3 to 2.25 μm , as well as a reference structure without a defect. Fig. 4(c) shows the resultant spectra. The dip in transmission centered on 4.5 μm is due to the main photonic stop gap of the woodpile photonic crystal lattice and agrees well with our calculations [Fig. 4(b)]. The striking feature which is apparent in all samples except the structure without a defect is a sharp peak within the stop gap region for $\Delta d = 0.6$ to 0.9 μm and again 1.5 to 2.25 μm constituting two successive cavity modes A and B, respectively. At a cavity size of 1.2 μm both modes are present simultaneously (Mode A at the upper gap edge in Fig. 4(b), Mode B at the lower one), although their appearance is less obvious as they are close to the gap edges. Fig. 4(d) compares the spectroscopy results (circles) with the eigenmode calculations (triangles). The shaded regions denote frequencies outside the bandgap, while the horizontal dotted line denotes the midgap frequency. The calculations reproduce the experimental results very well demonstrating the shift of both modes from the shorter to the longer-wavelength gap edge with increasing cavity size. As with typical quarter-wave stack Fabry-Perot filters our microcavities provide a first cavity mode at a cavity size of approximately a quarter-wave layer ($\Delta d=0.75 \mu\text{m}$) as well as a spacing between subsequent modes of 1.5 μm corresponding to half the light wavelength in the dielectric. The distributed feedback nature of the photonic crystal reflectors accounts for the order of magnitude smaller free spectral range compared to a simple Fabry-Perot etalon consisting of two reflective surfaces.

4. VOID-DOT-BASED 3D PHOTONIC CRYSTALS

4.1 Void dots generation in solid polymer

Comparing with void channels, void dots have much more flexibility to fabricate 3D photonic crystals with an arbitrary lattice. In order to view the fabricated void dots in the fabrication (longitudinal) direction, a cuboid bulk sample was prepared and 22 rows of void dots were fabricated at different depths with a dot spacing and a row spacing of $6\ \mu\text{m}$ and $3\ \mu\text{m}$, respectively, as illustrated in Fig. 5(a). After fabrication, the sample was rotated by 90 degrees and viewed by use of a confocal microscope (Fluoview, Olympus, Japan) [27]. Fig. 5 (b) shows the reflection (left) and transmission confocal images (right) of the void dots. Smooth and uniform void dots can be seen from the zoom-in transmission confocal images in Figs. 5 (c) and (d). Due to the weak spherical aberration caused by the refractive index mismatch between the polymer (1.56) and immersion oil (1.52) [28], the peak power at the focal point becomes lower at a deeper depth. As a result, the diameter of the dot decreases from approximately $1.8\ \mu\text{m}$ near the top surface down to approximately $1.2\ \mu\text{m}$ at a depth of $60\ \mu\text{m}$. It should be pointed out that the void dots are spherical which is different from the elliptical cross section of the fabricated rods in the two-photon polymerisation method [5]. The reason is that high-pressure gas generated during the microexplosion process in the void forces the voids to reshape to the most stable spherical shape.

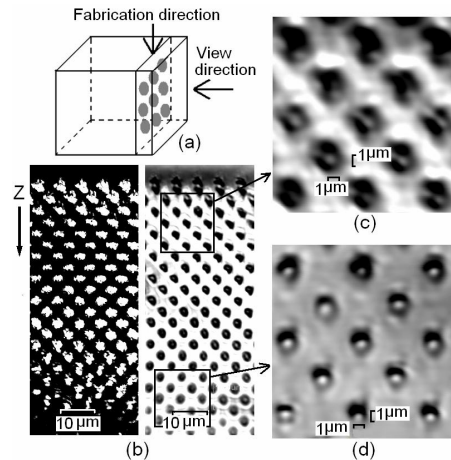


Fig. 5. Confocal reflection microscopy images of the top four layers [(a)-(d)] and the x-z scanning image of the top five layers (e). The sketch in upper-right corner shows the unit cell of the fcc lattice.

4.2 Photonic crystals with body-centred-cubic lattice

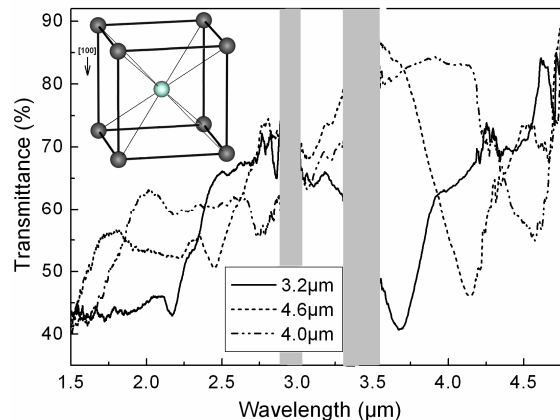


Fig. 6. Transmission spectra of bcc structures stacked in the [100] direction with lattice constants of $2.77\ \mu\text{m}$, $3.12\ \mu\text{m}$, and $3.46\ \mu\text{m}$. The first and second gaps are marked. The inset shows the sketch of a 3D bcc structure with a lattice spacing parameter of a and the stacking direction [100] marked by an arrow.

A body-centred-cubic (bcc) lattice is the second simplest lattice in the family of cubic lattices. As shown in the inset of Fig. 6, eight atoms locate at each corner and one atom locates at the centre of a cubic. 3D bcc photonic crystals consist of layers of voids with a square lattice with every second layer offsetting in x-, y-, z-directions by half of the lattice constant. Fig. 6 shows the transmission spectra of a 28-layer bcc structures stacked in the [100] direction with lattice constants of 2.77 μm , 3.12 μm and 3.46 μm , respectively. A suppression rate of ~ 50 for the fundamental gap has been achieved. One can also see an obvious higher order gap locating at the half wavelength of the fundamental gap.

4.3 Photonic crystals with face-centred-cubic lattice

A face-centred-cubic (fcc) lattice is a tightly packed structure and has a square arrangement in the [100] direction and a hexagonal (triangle) arrangement in the [111] direction. One can expect different angle dependence in the two directions. By stacking void dots layer by layer, we fabricated 3D structures with an fcc lattice in the [100] and [111] directions. The unit cell of an fcc lattice is schematically shown in the inset in Fig. 7. In the [100] direction, parallel planes of lattice points form a periodicity of two, offset by half of a lattice constant (a) in the x- or y-direction. Adjacent layers are spaced by half of a . In the [111] direction, the lattice points are packed in the pattern of a hexagonal-close-packed structure with a layer periodicity of three. The light penetrates through the photonic crystals perpendicular to the polymer film in both the fabrication process and the infrared transmission spectra measurement.

Fig. 7 shows the baseline-corrected transmission spectra of 28-layer 3D fcc void photonic crystals stacked in the [100] direction with the lattice constant of 3.4 μm , 4.0 μm and 4.96 μm , respectively. Two orders of stop gaps can be observed. The suppression rate of the transmission of the observed first order gap is as large as 74%. The observed second order gap located at exactly a half of the wavelength of the first order gap is also observed, with a suppression rate of approximately 20%. Both the first and second order gaps shift linearly to the longer wavelengths with an increase in the lattice constant [27].

Fig. 8 shows the baseline-corrected transmission spectra of 24-layer 3D fcc void photonic crystals stacked in the [111] direction with the lattice constant of 2.9 μm , 3.5 μm and 5.5 μm , respectively. The suppression rate of transmission of the observed main gaps is approximately 60%. The inset shows the mid-gap wavelengths of the first order gap as a function of lattice constants, which indicates a linear dependence. The linear fitting result shows a gradient of approximately 0.83. The transmission spectra of the photonic crystal with a lattice constant of 5.5 μm indicate the existence of a higher order stop gap at 2.2 μm , which is marked by an arrow. This gap should be the second order gap because it locates at approximately a half of the wavelength of the observed main gap (4.4 μm). Experimental results also showed that the angle dependence of the bandgap at different directions.

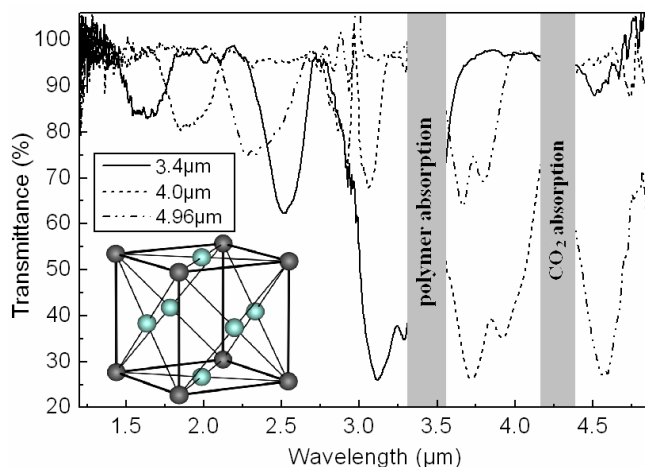


Fig. 7. Transmission spectra of 3D fcc void photonic crystals stacked in the [100] direction with lattice constants of 3.4 μm , 4.0 μm and 4.96 μm , respectively. The inset shows the sketch of a 3D fcc lattice.

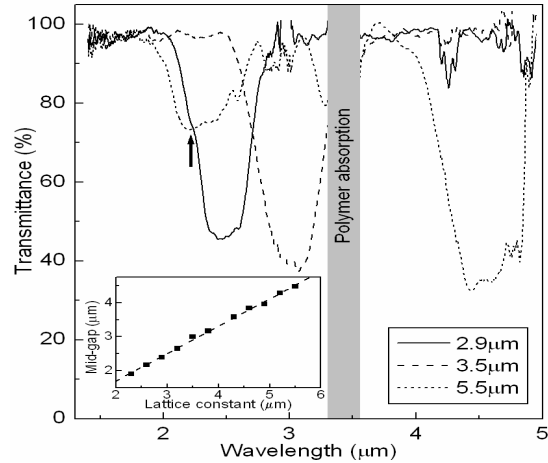


Fig. 8. Transmission spectra of 3D fcc structures stacked in the [111] direction with lattice constants of 2.9 μ m, 3.5 μ m and 5.5 μ m, respectively. The inset shows the relation of lattice constant and mid-gap position.

4.4 Photonic crystals with diamond lattice

In general, structures with a more spherical Brillouin zone are more likely to open 3D photonic bandgaps [29]. A diamond lattice with a layer periodicity of four is composed of two sets of fcc lattices offset by a quarter a in x -, y - and z -directions relative to each other. A diamond lattice fares much better than an fcc lattice for the following reasons. Firstly, the threshold value of the refractive index contrast to open a complete PBG is approximately 2 for a diamond lattice rather than 2.8 for an fcc lattice [30]. Secondly, a complete PBG appears between second and third bands for a diamond lattice rather than between eighth and ninth bands for an fcc lattice [31], which is therefore much stable against disorders and defects [32,33]. Thirdly, the bandgap is significantly larger for a diamond lattice [29]. In addition, according to the calculation, diamond photonic crystals with air spheres in a dielectric matrix can open a larger gap compared with the inverse one.

Fig. 9 shows the baseline-corrected transmission spectra of 32-layer 3D diamond void photonic crystals stacked in the [100] direction with the lattice constant of 4.12 μ m, 4.44 μ m and 4.72 μ m, respectively. The strong suppression rate of the observed first and second order gaps, approximately 65% and 75% respectively, indicates that the fabricated void spheres are well correlated each other. A linear relationship between the gap position and the lattice constant has been observed.

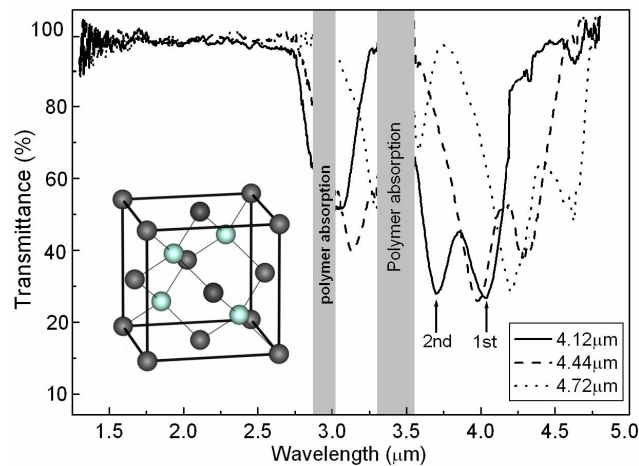


Fig. 9. Baseline-corrected transmission spectra of 3D void diamond photonic crystals stacked in the [100] direction with a lattice constant of 4.12 μ m, 4.44 μ m and 4.72 μ m. The insert shows the sketch of the diamond lattice.

5. CONCLUSIONS

We have generated micron-sized void channels and void dots inside a transparent solid polymer by using a femtosecond laser induced micro-explosion method. Due to the high-pressure gas inside the void cavities and the flexibility of the polymer, the surface of the void cavities is smooth and uniform. Void-channel based woodpile photonic crystals and void-dots based fcc, bcc and diamond photonic crystals have been fabricated. Substantial photonic bandgaps have been observed for all the fabricated structures. The properties of a functional Fabry-Perot planar cavity have been investigated in detail inside a channel-based photonic crystal. The experimental results prove that the femtosecond laser-induced micro-explosion method is an efficient method to fabricate 3D photonic crystals with arbitrary lattices.

ACKNOWLEDGEMENTS

This work was produced with the assistance of the Australian Research Council under the ARC Centres of Excellence Program. CUDOS (the Centre for Ultrahigh-bandwidth devices for Optical Systems) is an ARC Centre of Excellence.

REFERENCES

1. J. G. Fleming and S. Y. Lin, "Three-dimensional photonic crystal with a stop band from 1.35 to 1.95 μm ," *Opt. Lett.* 24, 49-51 (1999).
2. X. Wang, J. F. Xu, H. M. Su, Z. H. Zeng, Y. L. Chen, H. Z. Wang, K. P. Pang, and W. Y. Tam, "Three-dimensional photonic crystals fabricated by visible light holographic lithography," *Appl. Phys. Lett.* 82, 2212-2214 (2003).
3. R. C. Schroden, M. Al-Daous, C. F. Blanford, and A. Stein, "Optical Properties of Inverse Opal Photonic Crystals," *Chem. Mater.* 14, 3305-3315 (2002).
4. G. Subramanian, W. N. Manoharan, J. D. Thorne, and D. J. Pine, "Ordered Macroporous Materials by Colloidal Assembly: A Possible Route to Photonic Bandgap Materials," *Adv. Mater.* 11, 1261-1265 (1999).
5. M. Straub and M. Gu, "Near-infrared photonic crystals with higher-order bandgaps generated by two-photon photopolymerization," *Opt. Lett.* 27, 1824-1836 (2002).
6. B. H. Cumpston, S. P. Ananthavel, S. Barlow, D. L. Dyer, J. E. Ehrlich, L. L. Erskine, A. A. Heikal, S. M. Kuebler, I.-Y. S. Lee, D. McCord-Maughon, J. Qin, H. Röckel, M. Rumi, X.-L. Wu, S. R. Marder, and J. W. Perry, "Two-photon polymerization initiators for three-dimensional optical data storage and microfabrication," *Nature* 398, 51-54 (1999).
7. E. N. Glezer and E. Mazur, "Ultrafast-laser driven micro-explosions in transparent materials," *Appl. Phys. Lett.* 71, 882-884 (1997).
8. K. Yamasaki, S. Juodkazis, M. Watanabe, H. -B. Sun, S. Matsuo, and H. Misawa, "Recording by microexplosion and two-photon reading of three-dimensional optical memory in polymethylmethacrylate films," *Appl. Phys. Lett.* 76, 1000 (2000).
9. D. Day and M. Gu, "Formation of voids in a doped polymethylmethacrylate polymer," *Appl. Phys. Lett.* 80, 2404-2406 (2002).
10. M. J. Ventura, M. Straub, and M. Gu, "Void channel microstructures in resin solids as an efficient way to infrared photonic crystals," *Appl. Phys. Lett.* 82, 1649-1651 (2003).
11. M. Straub, M. Ventura, and M. Gu, "Multiple Higher-Order Stop Gaps in Infrared Polymer Photonic Crystals," *Phys. Rev. Lett.* 91 043901 (2003).
12. G. Zhou, M. Ventura, M. Straub, Min Gu, Atsushi Ono, S. Kawata, X. Wang, Y. Kivshar, "In-plane and out-of-plane bandgap properties of a two-dimensional triangular polymer-based void channel photonic crystal," *Appl. Phys. Lett.*, 84, 4415-4417 (2004).
13. M. Straub, M. Ventura and Min Gu, "Microvoid channel polymer photonic crystals with large infrared stop gaps and a multitude of higher-order bandgaps fabricated by femtosecond laser drilling solid resin," *Thin Solid Films* 453-454, 552-556 (2004).
14. J. D. Joannopoulos, *Photonic crystals: modeling the flow of light* (Princeton University Press, U.S.A., 1995).
15. S. G. Johnson and J. D. Joannopoulos, *Photonic crystals, the road from theory to practice* (Kluwer Academic Publishers, U.S.A., 2002).

16. A. Sharkawy, S. Shi, and D. W. Prather, "Multichannel wavelength division multiplexing with photonic crystals," *Appl. Opt.* 40, 2247-2252 (2001).
17. M. Koshiba, "Wavelength division multiplexing and demultiplexing with photonic crystal waveguide couplers," *J. Lightwave Technology* 19, 1970-1975 (2001).
18. B. Xu and H. Y. Ming, "Experimental observation of bistability and instability in a two-dimensional nonlinear optical superlattice," *Phys. Rev. Lett.* 71, 3959-3962 (1993).
19. S. F. Mingaleev and Y. S. Kivshar, "Nonlinear transmission and light localization in photonic-crystal waveguides," *J. Opt. Soc. Am. B* 19, 2241-2249 (2002).
20. M. Soljačić, C. Luo, J. D. Joannopoulos, and S. Fan, "Nonlinear photonic crystal microdevices for optical integration," *Opt. Lett.* 28, 637-639 (2003).
21. M. M. Beaky, J. B. Burk, H. O. Everitt, M. A. Haider, and S. Venakides, "Two-dimensional photonic crystal Fabry-Perot resonators with lossy dielectrics," *IEEE Trans. Microwave Theory Tech.* 47, 2085-2091 (1999).
22. H. B. Sun, V. Mizeikis, Y. Xu, S. Juodkazis, J. Y. Ye, S. Matsuo, and H. Misawa, "Microcavities in polymeric photonic crystals," *Appl. Phys. Lett.* 79, 1-3 (2001).
23. O. Painter, R. K. Lee, A. Scherer, A. Yariv, J. D. O'Brien, P. D. Dapkus, and I. Kim, "Two-dimensional photonic band-gap defect mode laser," *Science* 284, 1819-1821 (1999).
24. R. Ozaki, T. Matsui, M. Ozaki, and K. Yoshino, "Electrically color-tunable defect mode lasing in onedimensional photonic band-gap system containing liquid crystal," *Appl. Phys. Lett.* 82, 3593-3595 (2003).
25. S. H. Kim, H. Y. Ryu, H. G. Park, G. H. Kim, and Y. S. Choi, "Two-dimensional photonic crystal hexagonal waveguide ring laser," *Appl. Phys. Lett.* 81, 2499-2501 (2002).
26. E. Hecht and A. Zajac, *Optics* (Addison-Wesley Publishing Company, U.S.A., 2002), Chap. 9.
27. G. Zhou, M. J. Ventura, M. R. Vanner, and M. Gu, "Fabrication and characterization of face-centered-cubic void dots photonic crystals in a solid polymer material," *Appl. Phys. Lett.* 86, 011108 (2005).
28. D. Day and M. Gu, "Effects of Refractive-Index Mismatch on Three-Dimensional Optical Data-Storage Density in a Two-Photon Bleaching Polymer," *Appl. Opt.* 37, 6299-6304 (1998).
29. K. M. Ho, C. T. Chan, and C. M. Soukoulis, "Existence of a photonic gap in periodic dielectric structures," *Phys. Rev. Lett.* 65, 3152-3155 (1990).
30. H. S. Sözüer, J. W. Haus, and R. Inguva, "Photonic bands: Convergence problems with the plane-wave method," *Phys. Rev. B* 45, 13962-13972 (1992).
31. G. R. Yi and S. M. Yang, "Bandgap engineering of face-centered cubic photonic crystals made of hollow spheres," *J. Opt. Soc. Am. B* 18, 1156-1160 (2001).
32. Z. Y. Li and Z. Q. Zhang, "Fragility of photonic band gaps in inverse-opal photonic crystals," *Phys. Rev. B* 62, 1516-1519 (2000).
33. M.M. Sigalas, C. M. Soukoulis, C. T. Chan, R. Biswas, and K. M. Ho, "Effect of disorder on photonic band gaps," *Phys. Rev. B* 59, 12767-12770 (1999).